

Maximum Allowable Current Determination of RBS By Using a Directed Graph Model and Greedy Algorithm

Binghui Xu^{1†}, Guangbin Hua^{1†}, Cheng Qian^{1*}, Quan Xia^{1,2}, Bo Sun¹, Yi Ren¹, and
Zili Wang¹

¹School of Reliability and Systems Engineering, Beihang University, Beijing, 100191,
China

²School of Aeronautic Science and Engineering at Beihang University, Beijing, China

*Address correspondence to: cqian@buaa.edu.cn

[†]These authors contributed equally to this work.

Abstract

Reconfigurable battery systems (RBSs) present a promising alternative to traditional battery systems due to their flexible and dynamically changeable topological structure that can be adapted to different battery charging and discharging strategies. During RBS operation, a critical system parameter known as the maximum allowable current (MAC) become pivotal. This parameter is instrumental in maintaining the current of each individual battery within a safe range and serves as a guiding indicator for the system's reconfiguration, thereby ensuring its safety and reliability. This paper proposes a method to calculate the MAC of arbitrary RBSs using a greedy algorithm in conjunction with a directed graph model of the RBS. By introducing the shortest path of the battery, the greedy algorithm transforms the enumeration of switch states in the brute-force algorithm into the combination of the shortest paths, which greatly increases the efficiency with which the MAC is determined. The directed graph model, based on the equivalent circuit, provides a specific method for calculating the MAC of a given structure. The proposed method is validated on two published four-battery-RBSs and one with a more complex structure. The results are the same as those of the brute-force algorithm, but the proposed method significantly improves the computational efficiency ($N_s 2^{N_s - N_b} \log_{10} N_b$ times faster than the brute-force algorithm for an RBS with N_b batteries and N_s switches, theoretically). The main advantage of the proposed method is its ability to calculate the MAC of RBSs with arbitrary structures, even in scenarios with random isolated batteries.

1 Introduction

Battery energy storage systems (BESSs) are extensively used in various applications [1], such as wind power plants [2] and space power systems [3, 4], to store and release high-quality electrical energy [5].

Typically, a BESS consists of numerous batteries interconnected by series-parallel circuitry to provide the required capacity storage. However, traditional BESSs, in which the batteries are connected in a fixed topology, suffer from a significant weakness in their worst battery due to the so-called cask effect. Moreover, if the worst battery fails during operation, it is highly likely to exacerbate the degradation of the other batteries, leading to system-level reliability and safety issues [6, 7, 8]. These problems have become significant technical barriers in many engineering projects requiring high reliability, such as developing new-generation space vehicles [9]. Reconfigurable battery systems (RBSs), which can dynamically switch as required to different circuit topologies, are expected to solve those problem [10]. In a typical RBS, the extra switches are added between the batteries to form a reconfigurable network, where the circuit's topology can be changed by opening or closing the switches. The unhealthy batteries can be isolated from the system by opening the switches adjacent to them, thereby ensuring that the system remains in a reliable working mode [11]. Furthermore, the RBS can be reconfigured to adapt to different charging and discharging strategies, thereby improving the system's efficiency and extending the battery's life [12]. Those advantages make RBSs a promising alternative to traditional BESSs.

The early research on RBSs mainly focused on the topological design of the structure with different flexibility and reconfigurability to meet application requirements. For example, Ci et al. [13] proposed an RBS structure that dynamically adjusts the battery discharge rate to fully exploit the available capacity of each battery. Jan's [14, 15] structures reconfigure circuits with variant batteries in series to reach the constantly changing voltage requirements during electric vehicle charging. The structure proposed by Visairo et al. [16] changes the system's output voltage based on the load conditions, thereby reducing the power loss of the voltage regulator during the power supply process and improving the efficiency of energy use. Also, to enhance the energy efficiency of the system, Lawson et al. [17] and He et al. [18] proposed simplified structures that have fewer switches than Visairo's design. Kim et al. [19] improved the system's ability to recover from battery failures by introducing multiple ports into the structure. Those complex structures between batteries and switches give RBSs flexibility but also create the challenge in the design of the hardware. Current deviation and fluctuation occur when the system is reconfiguring. Specifically, when the system connect is swithed from series to parallel, circulating current between parallel cells can be triggered due to their voltage imbalance [20]. It will bring damage to the batteries, switches, and wires if not fully considered during the design of the RBSs. For instance, Engelhardt et al. [21] applied the RBS to a fast-charging scenario with adaptive cell switching, which can balance cell states while following the voltage request, but the switching of batteries leads to intolerant current variations. To solve this problem, Han et al. [22] derived an analytical expression for the maximum switch current during battery system reconfiguration. This helps guide the selection of switches and supports the design of RBS hardware.

Recently, more attention has been paid to the system state estimation and control of RBSs, and several approaches to optimize the system's performance have been proposed. The state estimation, one of the essential technologies of the traditional battery management system, is the premise of the system control, and shows great potential in the RBSs [23]. Couto et al. [24] proposed a partition-based unscented Kalman filter to estimate the state of a given large-scale RBS, using an

enhanced reduced-order electrochemical model. Kersten et al. [25] used the balancing current of neighboring cells in parallel operation to determine the battery impedances, yielding state of health and power capability. Schmid et al. [26] further taken advantage of the system's reconfigured characteristic to actively diagnose fault, whose algorithm changes the structure of the system in order to improve the fault isolability. Developing the effective control strategies of RBSs to achieve the optimal performance, such as better stability [27] and efficiency [28], is another hot research topic. Han et al. [29] proposed a near-fastest battery balancing algorithm to minimize the battery charge equalization time. Liu et al. [30] also proposed a maximum capacity utilization scheme based on a path planning algorithm to improve the battery consistency within the system. To break through the bottleneck of the potential short-circuit paths increase exponentially with the RBS's scale, Chen et al. [31] proposed a systematic approach based on sneak circuit theory. They thoroughly analyzed all paths between the cathode and anode of each battery in the RBS and identified paths that only contain switches as short-circuit paths for pre-checking before system reconfiguration. Furthermore, Artificial Intelligence also appears in the RBS management [32]. The effectiveness of deep reinforcement learning method has been validated on the real-world RBSs [28].

The maximum allowable current (MAC), defined as the maximum allowed current under the constraints of the battery cell, is a critical indicator of RBSs that needs to be evaluated during the design and control of the system. The MAC helps the designers assess whether the RBS meets the output current requirements and contributes to the formulation of appropriate and safe management strategies for the battery management system. Unfortunately, few studies have been proposed to determine the RBS MAC directly, owing to the complexity from reconfiguration. The computer science has the problem of scheduling tasks on dynamically reconfigurable hardware under the condition of limited resources and task interdependencies, similar to the MAC determination, and corresponding solution has been proposed [33, 34]. But it is hard to deal with the RBS's structural characteristics and circuit equations. From the perspective of RBS structure analysis, the MAC problem can be transformed into finding the maximum output current in all possible reconfigurations of the RBS. However, this may be an NP-hard problem [35]. Common methods, such as brute-force algorithm, simulated annealing (SA) algorithm and genetic algorithm (GA), have the disadvantages of inefficient, time-consuming, and cannot guarantee to obtain the global optimal solution.

To solve this issue, this paper proposes an efficient method to evaluate the MAC of RBSs. In this method, a greedy algorithm is designed to efficiently search the possible circuit topology of RBSs with MAC. This algorithm transforms the inefficiently searching reconfigurations into the proactively combining of the shortest paths of batteries. An improved direct graph model that considers the voltage, the internal resistance, the MAC of the battery, and the external load is also introduced to analyze the current of the RBS. The main contributions of this paper can be summarized as follows:

- An efficient method is proposed to determine the MAC of RBSs with arbitrary structures, including scenarios with isolated batteries.
- A greedy algorithm is applied to solve the MAC problem, the computational complexity of which is greatly reduced compared with the brute-force algorithm.
- An improved directed graph model is introduced to provide a specific method for calculating

113 the MAC of a given structure.

114 The remainder of this paper is organized as follows: Section II presents the framework and details
 115 of the proposed directed graph model and greedy algorithm. Section III discusses a case study that
 116 uses the proposed method to determine the MACs of two published four-battery RBSs and one with
 117 a more complex structure. The calculation results, the algorithm's computational complexity, and
 118 scenarios such as battery random isolation are also discussed. Finally, the concluding remarks are
 119 presented in Section IV.

120 2 Methodology

121 The central principle of this method is to connect the batteries in an RBS in parallel to the ex-
 122 tent possible, thereby maximizing the output current of the RBS. To achieve this universally and
 123 automatically, the overall process is divided into the four steps shown in Fig. 1. First, a directed
 124 graph model is established for subsequent computations. The model not only contains the con-
 125 nected relationships between batteries and switches but also retains the performance parameters of
 126 the batteries. Subsequently, based on the equivalent circuit, the MAC problem is transformed into
 127 specific objective functions and constraints. The shortest paths (SPs, where additional batteries
 128 and switches on the path are penalized as distance) for the batteries are then obtained by using the
 129 Dijkstra algorithm to connect the batteries in the RBS in parallel. Finally, a greedy algorithm is
 130 used to organize the switches, allowing the batteries to connect via their SPs while satisfying the
 131 constraints, resulting in the MAC of the RBS.

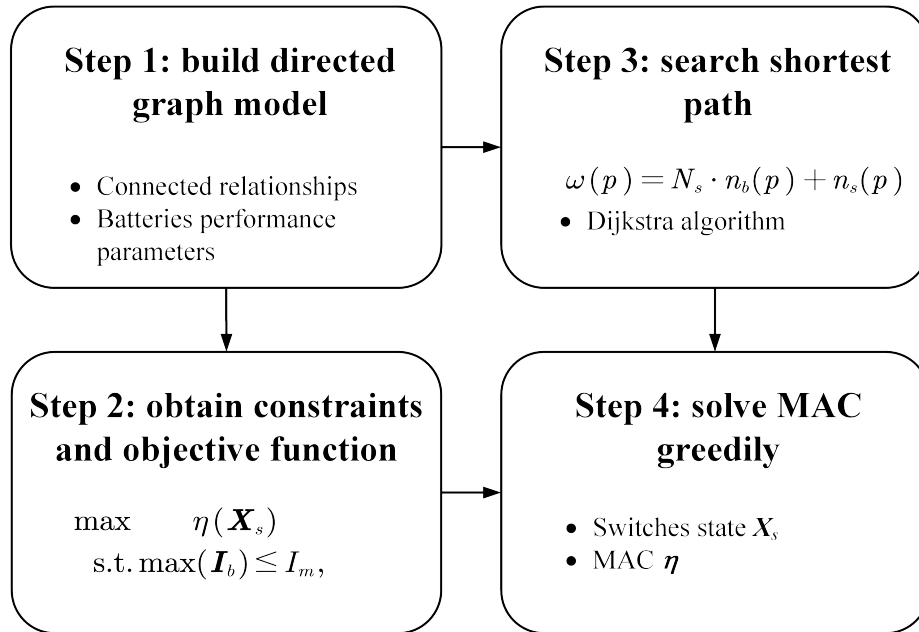


Figure 1: Diagram of this method, which contains four main steps.

2.1 Directed graph model

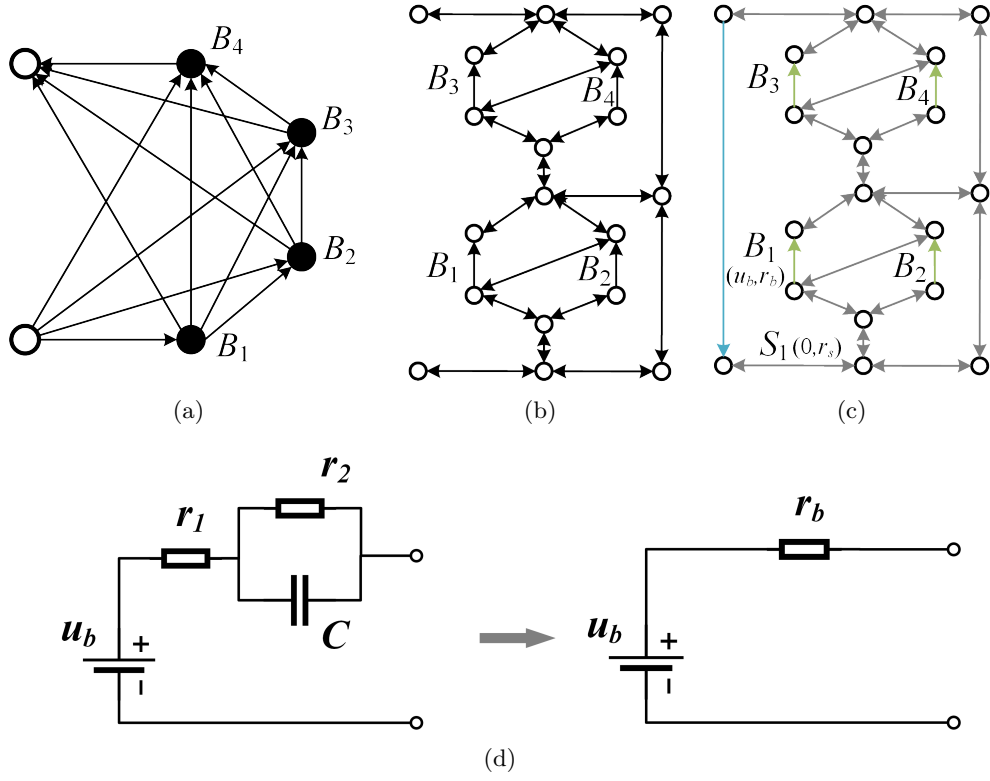


Figure 2: Directed graph models used in (a) He’s work [36], (b) our previous work, and (c) the improved model in this paper. (d) The equivalent circuit of a battery in this method.

He et al. [36] proposed an abstracted directed graph model for an RBS, where the nodes represent the batteries, the edges represent the configuration flexibility, and the weight of each vertex corresponds to the battery voltage (Fig. 2a). The model captures all potential system configurations and offers a direct metric for configuration flexibility, but it does not specify the physical implementation of the connectivity between batteries, meaning that one graph might correspond to multiple RBS structures. We previously proposed a directed graph model that differs completely from He’s model by using nodes to represent the connections between batteries and switches and directed edges to represent batteries and switches (Fig. 2b), allowing for a one-to-one correspondence between the RBS structure and the directed graph model. This model accurately and comprehensively represents the RBS topological structure but cannot be used for quantitative MAC calculations because it does not consider the voltage, internal resistance, and MAC of the battery. To address this issue, we improve our previous model by adding electromotive force and resistance attributes on the edges based on its equivalent circuits. The model also considers the external load as an equivalent resistance and integrates it into the analysis, making it a complete circuit model for later circuit analyses. Fig. 2c shows the improved directed graph model used in this paper. The following provides a detailed explanation of the method for equating components in RBSs and constructing the directed graph

model.

To use circuit analysis methods to solve the MAC of the RBS, the components in the RBS are equated to ideal circuit elements. For instance, as shown in Fig. 2d, the battery in the RBS is represented as a black-box circuit consisting of two resistors r_1 and r_2 and a capacitor C , known as the Thevenin model [37, 38]. With an emphasis on the stable output of the RBS, the capacitor in the Thevenin model can be considered as an open circuit without affecting the steady-state current. Therefore, battery B_i in the RBS can be simplified as a series connection between a constant voltage source u_i and a resistor r_i . Furthermore, the state of switch S_j in the RBS is represented by a binary variable x_j , where 0 is ON and 1 is OFF. When the switch is closed, the circuit can be regarded as a resistor with a very small resistance r_j . Finally, the external load is considered as a resistor with resistance R_o .

For a given RBS structure, its directed graph model $G(V, E)$ is constructed as follows:

1. Nodes: The nodes in the directed graph correspond to the connection points of components in the actual RBS. Assuming there are a total of N nodes in the RBS, for the sake of convenience, the anode of the RBS is denoted as v_1 and the cathode as v_N .
2. Edges: The edges in the directed graph correspond to the batteries, switches, and external electrical loads in the actual RBS. Therefore, there are three types of directed edges. For battery B_i , its directed edge e_i is drawn from the cathode to the anode because the battery in operation only allows current to flow in one direction. For switch S_j , since it is allowed to work under bidirectional currents, it is represented by a pair of directed edges with two-way directions. Regarding the external electronic load, because it is connected to the anode and cathode of the RBS, a directed edge from v_N to v_1 represents it. In conclusion, for a given RBS structure with N_b batteries and N_s switches, the number of directed edges is $N_b + 2N_s + 1$, where 1 refers to the external electrical load.
3. Attributes of edges: Each edge is assigned two attributes, voltage difference and resistance, based on the equivalent method mentioned above. The values for battery B_i , switch S_j , and external loads correspond to (u_i, r_i) , $(0, r_j)$, and $(0, R_o)$, respectively.

2.2 Constraints and objective function

For a given RBS, determining its MAC involves maximizing the RBS output current while ensuring that all battery currents do not exceed the batteries' MAC. This subsection establishes the constraints and objective function to determine the RBS's MAC through circuit analysis based on the directed graph model provided in the previous section.

First, the topology in the directed graph model is represented in matrix form \mathbf{A} , known as the incidence matrix and defined as follows:

$$a_{kl} = \begin{cases} 1, & \text{edge } l \text{ leaves node } k, \\ -1, & \text{edge } l \text{ enters node } k, \\ 0, & \text{otherwise.} \end{cases} \quad (1)$$

For a directed graph consisting of N nodes and $N_b + 2N_s + 1$ directed edges, its incidence matrix \mathbf{A} is an $N \times (N_b + 2N_s + 1)$ matrix. In this matrix, the rows and columns represent the nodes and edges of the directed graph, respectively. By distinguishing the components in the RBS corresponding to each column, \mathbf{A} can be rewritten as

$$\mathbf{A} = \begin{bmatrix} \mathbf{A}_b & \mathbf{A}_s & \mathbf{A}_o \end{bmatrix}, \quad (2)$$

where \mathbf{A}_b , \mathbf{A}_s , and \mathbf{A}_o are the submatrices corresponding to the batteries, switches, and external electrical load, respectively. To reduce the computational complexity, the dimensions of matrix \mathbf{A} are reduced. Since each directed edge has one node to leave and one to enter, the values in every column of \mathbf{A} sum to zero. Therefore, removing the last row will not result in a loss of information. Conversely, since each switch in the RBS is represented by a pair of directed edges with two-way directions, the two columns corresponding to the switch are mutually opposite. Thus, for the submatrix \mathbf{A}_s , only one column is retained for each pair of columns representing the same switch. As a result, \mathbf{A} can be reduced to an $(N - 1) \times (N_b + N_s + 1)$ matrix, denoted $\tilde{\mathbf{A}}$, for further calculation of current and voltage. Similar to Eq. (2), $\tilde{\mathbf{A}}$ can be rewritten as

$$\tilde{\mathbf{A}} = \begin{bmatrix} \tilde{\mathbf{A}}_b & \tilde{\mathbf{A}}_s & \tilde{\mathbf{A}}_o \end{bmatrix}. \quad (3)$$

After obtaining the incidence matrix, the currents of all batteries and output in the RBS are determined by solving the circuit equations. According to Kirchhoff's laws, we have

$$\begin{cases} \tilde{\mathbf{A}}\mathbf{I} = \mathbf{0}, \\ \mathbf{U} = \tilde{\mathbf{A}}^T \mathbf{U}_n, \end{cases} \quad (4)$$

where \mathbf{I} and \mathbf{U} indicate the current and voltage difference arrays of the $N_b + N_s + 1$ edges, respectively, and \mathbf{U}_n is the voltage array of the $N - 1$ nodes. These directed edges are treated as generalized branches and expressed in matrix form as follows:

$$\mathbf{I} = \mathbf{Y}\mathbf{X}\mathbf{U} - \mathbf{Y}\mathbf{X}\mathbf{U}_s + \mathbf{I}_s, \quad (5)$$

where \mathbf{U}_s and \mathbf{I}_s denote the source voltage and source current of the generalized branches, respectively. Because all batteries have been equivalent to voltage sources rather than current sources in the previous subsection, all elements of the array \mathbf{I}_s are zero, whereas the elements of the array \mathbf{U}_s are equal to the first attribute of the corresponding edges in the directed graph. The matrix \mathbf{Y} in Eq. (5) is the admittance matrix of the circuit and is defined as the inverse of the impedance matrix. The elements on the diagonal of matrix \mathbf{Y} are equal to the reciprocal of the resistance, which is the second attribute of the corresponding edges in the directed graph. The off-diagonal elements of \mathbf{Y} are zero. \mathbf{X} is the state matrix that determines whether the RBS batteries and switches can pass

209 current. It is defined as

$$\mathbf{X} = \text{diag}(\underbrace{1, 0, \dots, 1}_{N_b \text{ of } 0/1}, \underbrace{1, 0, \dots, 1}_{N_s \text{ of } 0/1}, 1) = \begin{bmatrix} \mathbf{X}_b & & \\ & \mathbf{X}_s & \\ & & 1 \end{bmatrix}, \quad (6)$$

210 where element x_i of matrix \mathbf{X}_b indicates whether battery B_i has been removed from the circuit,
 211 with $x_i = 1$ indicating removal and $x_i = 0$ indicating that battery B_i is still available to supply
 212 power. When all batteries are healthy and capable of providing current to the external load, \mathbf{X}_b
 213 is the identity matrix. The elements x_j of matrix \mathbf{X}_s determine whether switch S_j is closed, with
 214 $x_j = 1$ indicating a closed switch and $x_j = 0$ indicating an open switch, which is consistent with the
 215 previous subsection.

216 Theoretically, the output current I_o and the currents of each battery \mathbf{I}_b in the RBS can be
 217 determined by solving Eqs. (4)–(6) under any given state \mathbf{X} . To further simplify the problem, it
 218 is assumed that all batteries have the same electromotive force and internal resistance, which are
 219 denoted u_b and r_b , respectively. This allows us to derive explicit expressions for I_o and \mathbf{I}_b . After
 220 derivation and simplification, the output current I_o and the currents of each battery \mathbf{I}_b are ultimately
 221 represented as Eqs. (7) and (8), respectively:

$$I_o = \frac{1}{R_o r_b} \tilde{\mathbf{A}}_o^T \mathbf{Y}_n^{-1}(\mathbf{X}) \tilde{\mathbf{A}}_b \mathbf{U}_b, \quad (7)$$

$$\mathbf{I}_b = \frac{1}{r_b^2} [\tilde{\mathbf{A}}_b^T \mathbf{Y}_n^{-1}(\mathbf{X}) \tilde{\mathbf{A}}_b \mathbf{U}_b - r_b \mathbf{U}_b], \quad (8)$$

223 where \mathbf{U}_b is an $N_b \times 1$ array with all elements equal to u_b , and \mathbf{Y}_n is the equivalent admittance
 224 matrix of the circuit and is defined as

$$\mathbf{Y}_n(\mathbf{X}) = \frac{1}{R_o} \tilde{\mathbf{A}}_o \tilde{\mathbf{A}}_o^T + \frac{1}{r_b} \tilde{\mathbf{A}}_b \mathbf{X}_b \tilde{\mathbf{A}}_b^T + \frac{1}{r_s} \tilde{\mathbf{A}}_s \mathbf{X}_s \tilde{\mathbf{A}}_s^T. \quad (9)$$

225 To characterize the current output capacity of the RBS structure under different switching states,
 226 an indicator η is defined by the ratio of I_o to $\max(\mathbf{I}_b)$:

$$\eta = \frac{I_o}{\max(\mathbf{I}_b)}. \quad (10)$$

227 Finally the problem of finding the MAC can be formulated as

$$\max \eta(\mathbf{X}_s) \quad (11)$$

$$\text{s.t. } \max(\mathbf{I}_b) \leq I_m, \quad (12)$$

228 where I_m is the MAC of the battery.

229 However, it remains computationally difficult to solve Eq. (11) because of \mathbf{Y}_n^{-1} . On one hand,
 230 the introduction of nonlinear terms by \mathbf{Y}_n^{-1} renders many methods in linear optimization unsuitable
 231 for this problem. On the other hand, the rank of \mathbf{Y}_n is proportional to the number of batteries and

switches, which can be very large for a large RBS, leading to a significant computational burden. As a result, intelligent algorithms that rely on evolution by iteration may face efficiency problems when dealing with a large RBS. To address this issue, the problem should be considered from the perspective of guiding the RBS to reconstruct as many parallel structures as possible. Consequently, a greedy algorithm based on the shortest path is proposed. The detailed implementation of this algorithm is presented in the following two subsections.

2.3 Shortest path

The path p used in this method is defined as the complete route that passes through one battery (or a consecutive series of batteries) and closed switches, connecting the anode v_1 to the cathode v_N of the RBS. By applying a penalty to the series-connected batteries on the path, where additional batteries imply a greater distance, the algorithm encourages the RBS to form parallel structures to the extent possible. In addition, to reduce the number of switches controlled during the reconstruction process, a penalty is also applied to the total number of switches on the path while ensuring the minimum number of batteries. Therefore, the distance ω of path p is

$$\omega(p) = N_s n_b(p) + n_s(p), \quad (13)$$

where N_s is the total number of switches in the system, and $n_b(p)$ and $n_s(p)$ are number of batteries and switches in path p , respectively. Moreover, the shortest path SP_i is defined as the path with the minimum ω for battery B_i :

$$SP_i = \arg \min_{p \in P_i} \omega(p), \quad (14)$$

where P_i is the set of all paths from v_1 to v_N that pass through directed edge i .

SP_i can be solved by the Dijkstra algorithm. The Dijkstra algorithm is a graph-search method that finds the shortest path between two given nodes in a weighted graph, efficiently solving the single-source shortest-path problem. Denoting the cathode and anode of battery B_i as v_i^- and v_i^+ respectively, then path p of battery B_i can be divided into three segments: $v_1 \rightarrow v_i^-$, $v_i^+ \rightarrow v_N$, and $v_i^- \rightarrow v_i^+$. $v_i^- \rightarrow v_i^+$ is the directed edge corresponding to battery B_i . With the Dijkstra algorithm, shortest paths for $v_1 \rightarrow v_i^-$ and $v_i^+ \rightarrow v_N$ can be calculated under the weights given in Eq. (13) and denoted $SP(v_1 \rightarrow v_i^-)$ and $SP(v_i^+ \rightarrow v_N)$, respectively. Finally, SP_i for battery B_i is formed by the complete path, which consists of $SP(v_1 \rightarrow v_i^-)$, $v_i^- \rightarrow v_i^+$, and $SP(v_i^+ \rightarrow v_N)$.

2.4 Greedy algorithm

From the perspective of series vs parallel connections, integrating more batteries into the circuit through their shortest paths (SPs) results in more batteries connected in parallel, thereby increasing the total output current of the RBS. However, conflicts may arise between the SPs of different batteries. For instance, the SPs of two batteries might form a short-circuit RBS structure, which is not allowed. To address this issue, a greedy algorithm incorporates as many SPs as possible while satisfying the reconstruction requirements.

265 The algorithm (see pseudo-code in Algorithm 1) is illustrated in Fig. 3 and is summarized as
 266 follows: First, the SPs are obtained by using Eqs. (13) and (14) in conjunction with the Dijkstra
 267 search. Next, the matrix \mathbf{A} is calculated using Eq. (1), and the initial N_{set} is set to N_b . The
 268 algorithm uses a dichotomy method to iteratively check until convergence different combinations of
 269 c_b batteries from N_b and updates N_{set} . For each combination, the algorithm constructs an effective
 270 solution if possible and calculates the currents I_o and I_b by using Eqs. (7) and (8). If the maximum
 271 current I_b is less than or equal to I_m , η is calculated by using Eq. (10), and the maximum η is
 272 updated accordingly. Finally, the algorithm outputs the maximum η once N_{set} converges.

273 3 Case Study

274 3.1 Structures and details

275 Currently, two types of RBS structures have been proposed by Visairo et al. [16] and Lawson et
 276 al. [17], both of which have seen real use. The primary goal of Visairo’s structure (Fig. 4b) is
 277 to dynamically adjust the RBS output power. However, the isolation of unhealthy batteries is not
 278 sufficiently addressed in their work. Lawson et al. designed the RBS structure shown in Fig. 4a
 279 to isolate batteries. Although this structure easily isolates batteries, it cannot dynamically adjust
 280 the output current of the RBS. Based on the structures of Visairo and Lawson, this paper proposes
 281 the structure shown in Fig. 4c. By integrating the Visairo RBS structure into the Lawson RBS
 282 structure, the proposed structure not only has the flexibility to switch the batteries between series,
 283 parallel, and mixed series-parallel modes but also allows the isolation of highly degraded batteries
 284 from the RBS.

285 In the case study, these RBS systems are investigated and compared: (a) three different structures
 286 (Figs. 4a–4c) with the same four batteries; (b) the same structure in Figs. 4c with two/four/six
 287 batteries; and (c) the four-battery structure in Figs. 4c with random isolated batteries. The greedy
 288 algorithm proposed in this work is also compared with the brute-force algorithm, SA, and GA to
 289 validate its effectiveness and efficiency. In order to adapt the two heuristic algorithms to the system’s
 290 structure and scale, the number of the state neighbours of SA and the population size of GA are
 291 both set to $N_b \cdot N_s$, which increase with the number of batteries and switches in the system. The
 292 other algorithms’ parameters are shown in Tab. 1.

Table 1: Algorithms parameters of SA and GA.

Algorithm/paramter	Value
SA/initial temperature	100
SA/final temperature	1
SA/cooling rate	0.95
GA/total generations	100
GA/crossover probability	0.8
GA/mutation probability	0.02

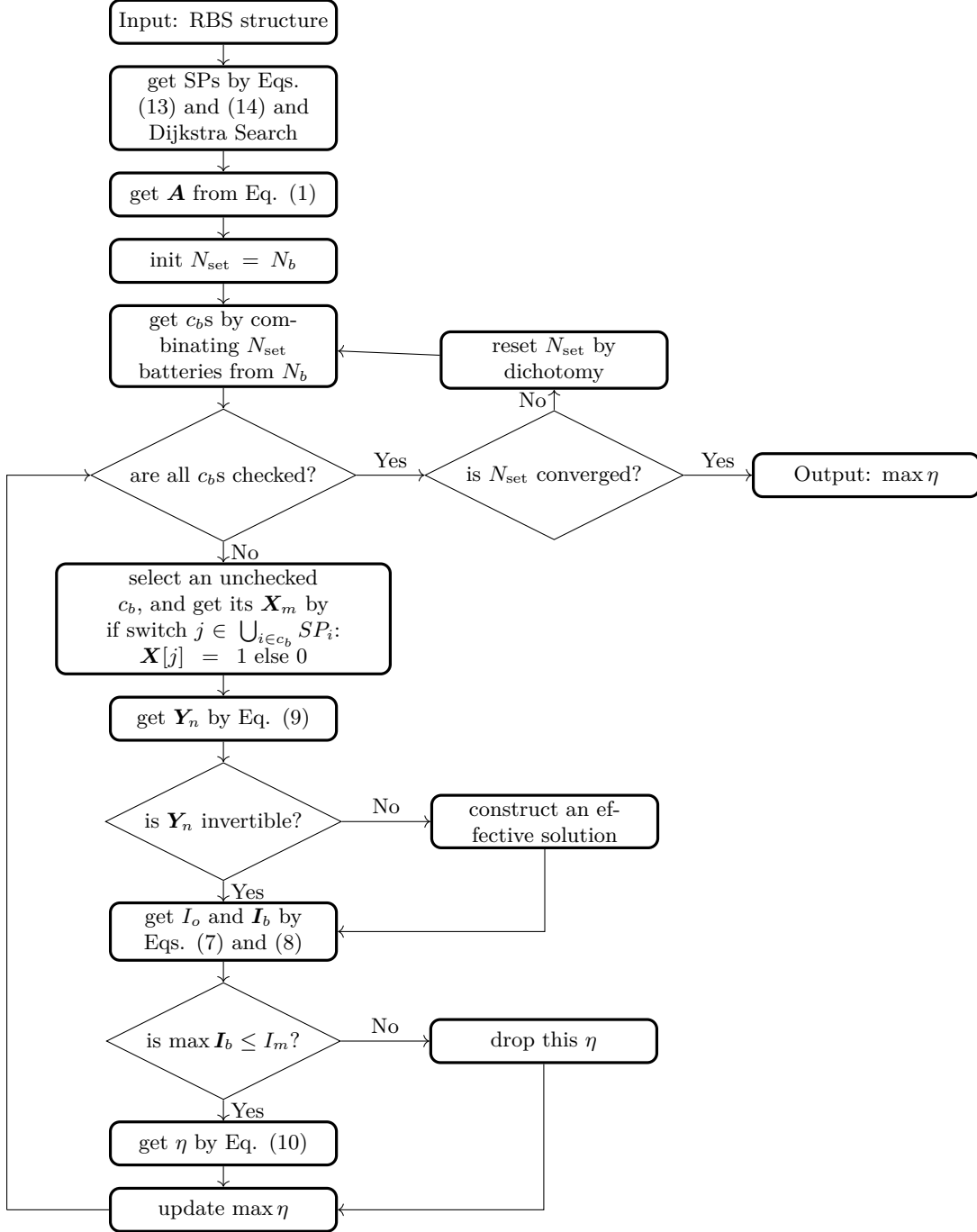


Figure 3: The computational flowchart of the MAC for a given RBS.

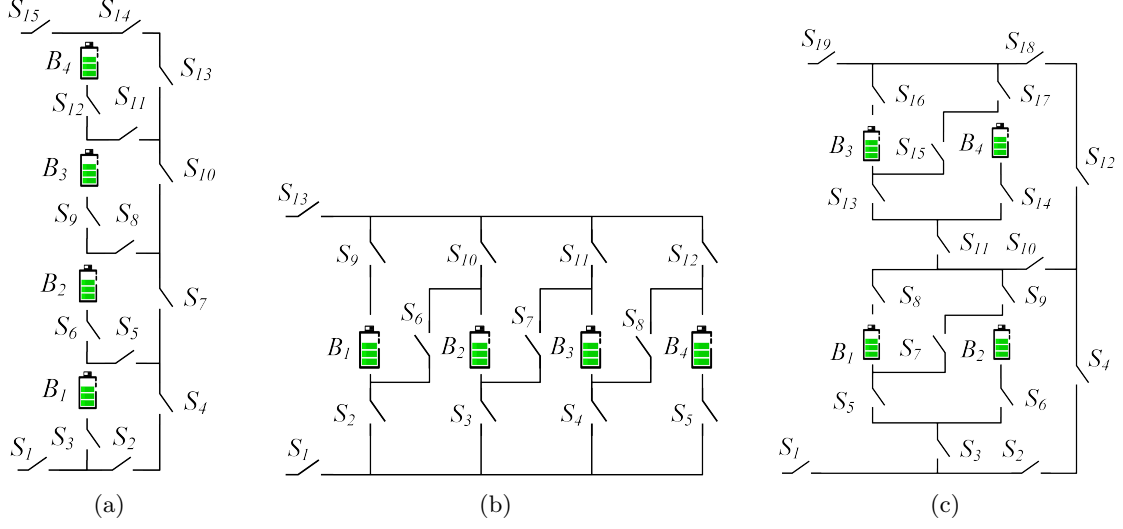


Figure 4: The four-battery RBS structures proposed by (a) Lawson [17], (b) Visairo [16], and (c) this paper.

3.2 Result

3.2.1 the shortest path

Using Eq. (13) and the Dijkstra algorithm, the SPs of the four batteries in the RBS structures of Figs. 4a, 4b, and 4c are calculated and highlighted with difference colors in Figs. 5a, 5b, and 5c, respectively.

3.2.2 three structures with four batteries

After obtaining the SPs, the MACs of the three RBS structures with four batteries are calculated using the proposed greedy algorithm, and the results are shown in Tabs. 2, 3, and 4, each of which contains the states of the switches, the output current I_o , the battery current I_b , and the ratio η when the system output reaches the MAC. The correspond switch-control schemes are shown as blue-highlighted electric current in Figs. 6a, 6b, and 6c, respectively. To verify and compare the proposed greedy algorithm, we also used the brute-force algorithm, which iterates through all possible switch states, and the heuristic algorithms (SA and GA) to calculate the MAC of the same RBSs. The final results of the brute-force algorithm are the same as the ones of the greedy algorithm, which are shown in Tabs. 2, 3, and 4. But, the brute-force algorithm counts all possible switch states, which equates to 2^{15} , 2^{13} , and 2^{19} structures, respectively. The two heuristic algorithms' temporal evaluation of the objective values during the iteration process are shown in Figs. 7a, 7b, and 7c, respectively, compared with the proposed greedy algorithm.

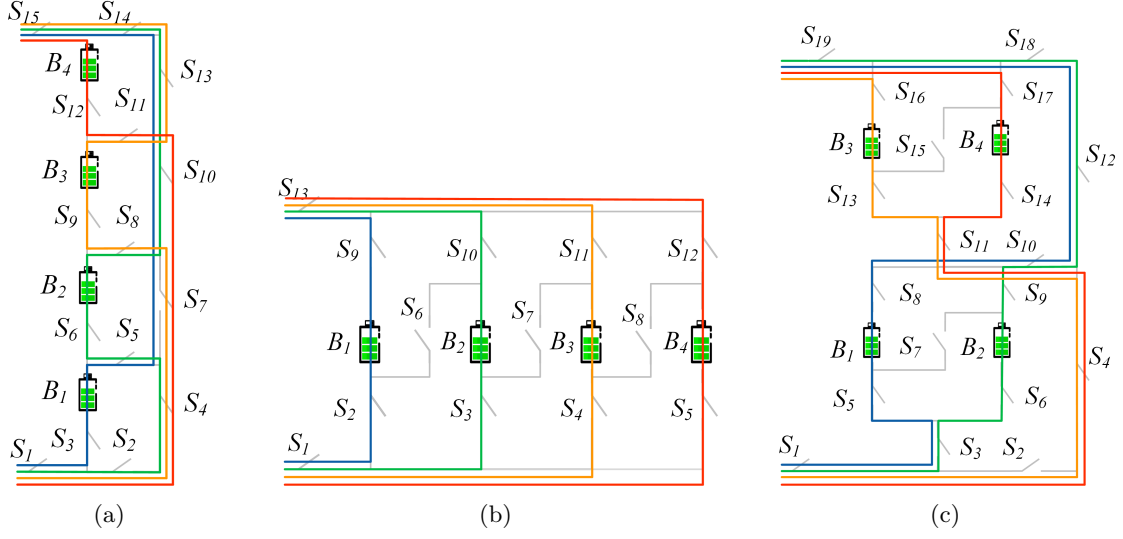


Figure 5: The SPs of the four batteries in the RBS structures of (a) Fig. 4a, (b) Fig. 4b, and (c) Fig. 4c.

Table 2: MAC Calculating result of the four-battery RBS structure in Fig. 4a.

Structure	Figure 4a with 4 batteries and 15 switches
Switch ON	$S_1, S_3, S_5, S_7, S_{10}, S_{13}, S_{14}, S_{15}$
I_o	$u_b / (R_o + r_b)$
\mathbf{I}_b	$[u_b / (R_o + r_b), 0, 0, 0]$
$\max \eta$	1

Table 3: MAC Calculating result of the four-battery RBS structure in Fig. 4b.

Structure	Figure 4b with 4 batteries and 13 switches
Switch ON	$S_1, S_2, S_3, S_4, S_5, S_9, S_{10}, S_{11}, S_{12}, S_{13}$
I_o	$4u_b / (4R_o + r_b)$
\mathbf{I}_b	$[u_b / (4R_o + r_b), u_b / (4R_o + r_b), u_b / (4R_o + r_b), u_b / (4R_o + r_b)]$
$\max \eta$	4

Table 4: Calculated MAC for four-battery RBS structure in Fig. 4c.

Structure	Figure 4c with four batteries and 19 switches
Switch on	$S_1, S_3, S_5, S_6, S_8, S_9, S_{10}, S_{12}, S_{18}, S_{19}$
I_o	$2u_b / (2R_o + r_b)$
\mathbf{I}_b	$[u_b / (2R_o + r_b), u_b / (2R_o + r_b), 0, 0]$
$\max \eta$	2

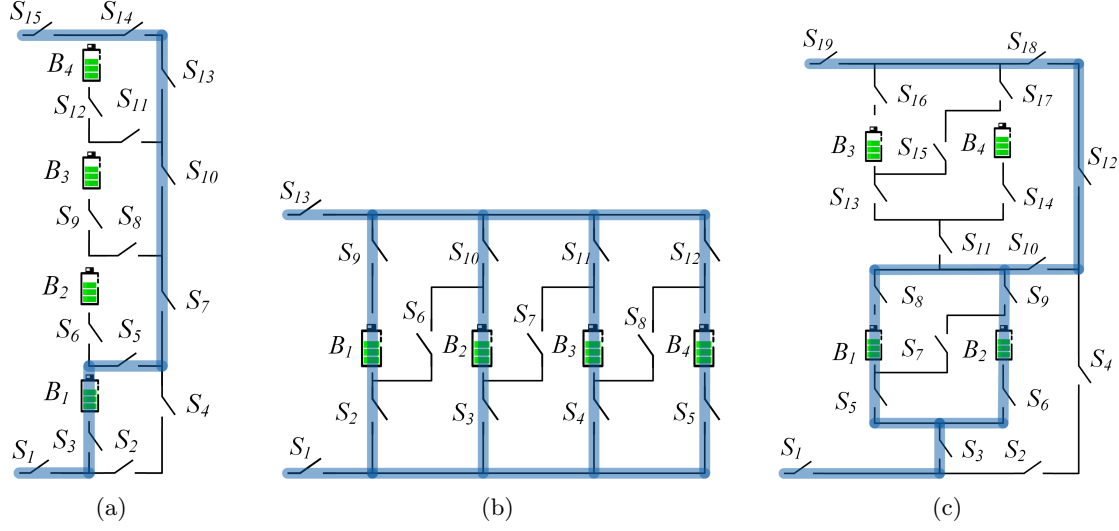


Figure 6: The RBSs' switch-control schemes with the output reaching the MAC.

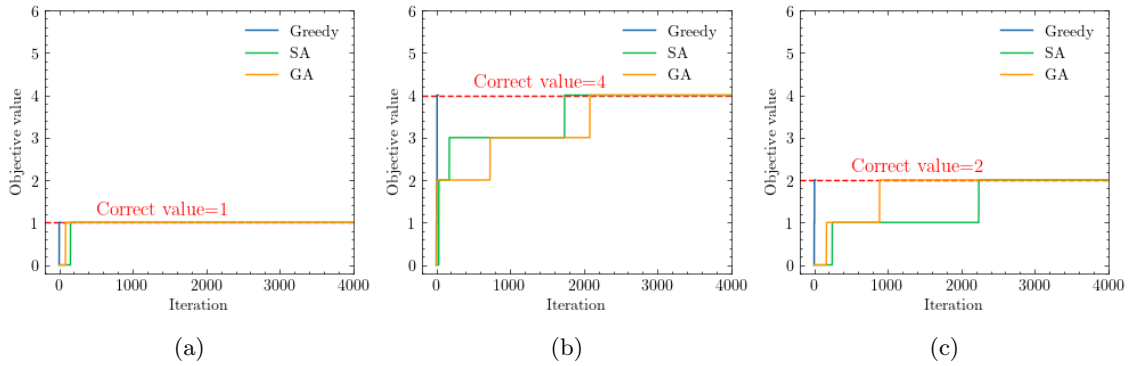


Figure 7: The temporal evolution of the objective values during the iteration process of calculating the RBS structures in (a) Fig. 4a, (b) Fig. 4b, and (c) Fig. 4c

3.2.3 structures with different numbers of batteries

We next consider the RBS structure in Fig. 4c with two, four, and six batteries. The result of four-battery structure has been shown in Tab. 4, Figs. 6c, and 7c. The structures and final switch-control schemes of the remaining two-battery and six-battery systems are illustrated in Figs. 8a and 8b, respectively. And the temporal evolution of the objective values throughout the iteration process are shown in Figs. 9a and 9b, respectively.

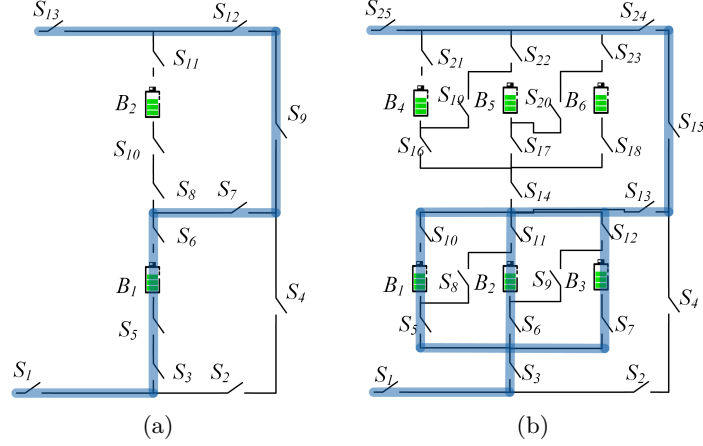


Figure 8: The (a) two-battery and (b) six-battery RBSs' switch-control schemes with the output reaching the MAC.

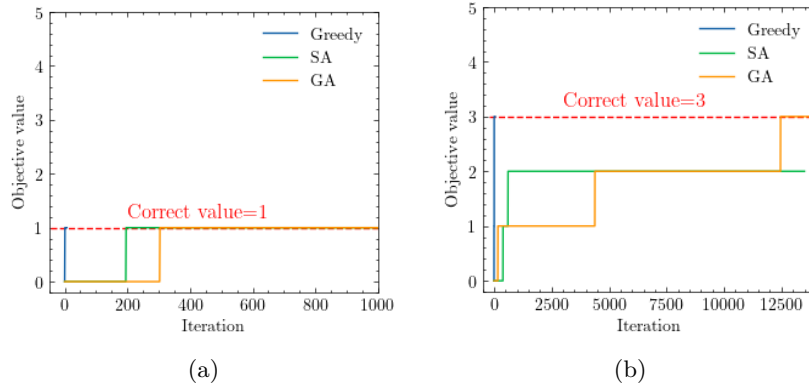


Figure 9: The temporal variation of the objective values during the iteration process of calculating the RBS structures in (a) Fig. 8a and (b) Fig. 8b.

3.2.4 random isolated batteries

To assess the effectiveness of the proposed algorithm in the scenario of unhealthy batteries, the RBS with random isolated batteries is also taken into account and computed. In the case of the four-battery RBS structure depicted in Fig. 4c, there are four possible scenarios of isolated batteries: (a) only one unhealthy battery, (b) two unhealthy batteries that are separated in the two substructure,

322 (c) two batteries located in the same substructure, and (d) three batteries. The resulting MAC
 323 (η) values for these four scenarios are 2, 2, 1, and 1, respectively. Furthermore, the corresponding
 324 switch-control schemes for these four scenarios are illustrated in Figs 10a–10d.

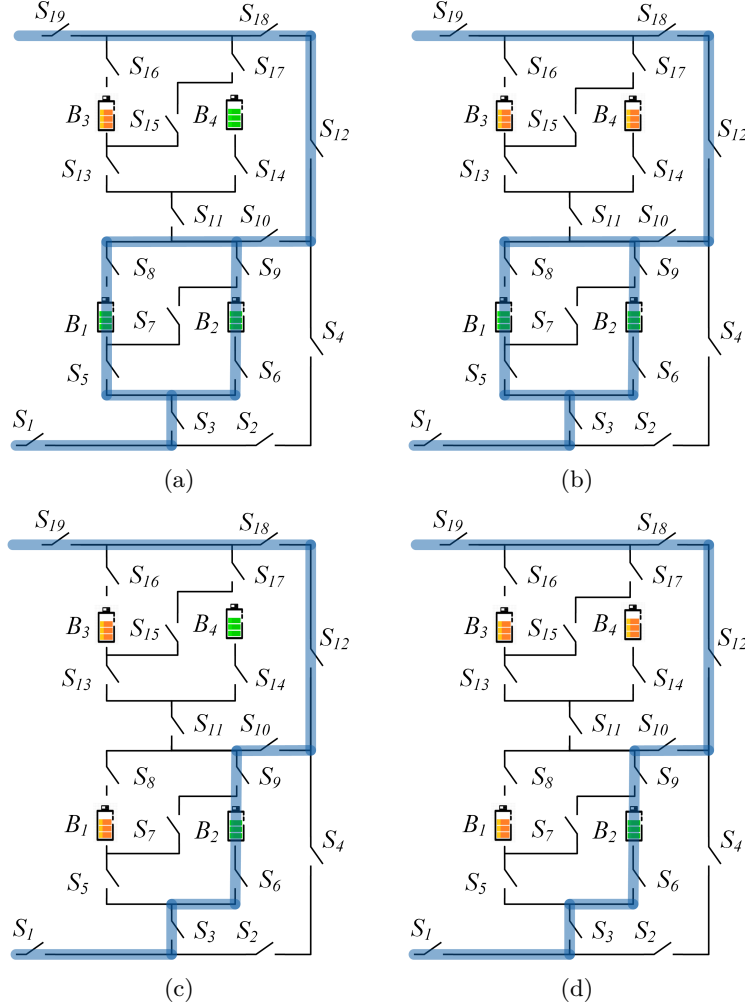


Figure 10: Circuit states of MACs when isolating (a) one, (b) two (in different substructures), (c) two (in the same substructure), and (d) three batteries for the structure in Fig. 4c.

3.3 Discussion

3.3.1 correctness of the results

The correctness of the outcomes provided by the proposed greedy algorithm will be discussed from two perspectives: circuit analysis and validation against the brute-force algorithm. Let's take the four-battery RBS structure shown in Fig. 4c as an example. When B_1 and B_2 or B_3 and B_4 are connected in parallel, the RBS produces the maximum current, which is $\eta = 2$ (i.e., twice the current output of a single battery in the RBS). Adding more batteries to the main circuit only creates a

series structure and does not improve the MAC. Therefore, the switch-control scheme provided in Tab. 4 maximizes the RBS output current. On the other hand, the brute-force method, which examines all possible switch states, also yields the same η . This indicates that the proposed greedy algorithm successfully identifies the MAC among all the potential reconfigured structures.

3.3.2 advantages and disadvantages of our method

The proposed greedy algorithm possesses a significant advantage in terms of its effectiveness and efficiency. In this paper, it is compared with the brute-force algorithm, SA, and GA. While the brute-force algorithm ensures the correctness of the results by exploring all possible switch states, it comes at a high computational cost. The SA and GA are commonly used heuristic algorithms for addressing NP-hard problems. They selectively generate solutions for the switching states to maximize the objective value η . However, neither of these two algorithms can determine whether the current η represents the final MAC or if they should continue searching for better solutions. Moreover, as depicted in Figs. 7a–7c and Figs. 9a–9b, the SA and GA algorithms require more iterations to converge to the final solution compared to the proposed greedy algorithm. In contrast, the proposed greedy algorithm can identify the correct MAC in a shorter number of steps.

To further elaborate on the efficiency of our algorithm, we analyze the time complexity of both the brute-force algorithm and the greedy algorithm. If an RBS has N_b batteries and N_s switches and the corresponding directed graph has N nodes, 2^{N_s} iterations are required to traverse all reconfigured structures. Calculating each reconfigured structure using Eqs. (7)–(10) requires matrix inversion and matrix multiplication, which has a time complexity of $O(N^3 + 2N^2N_b + N^2N_s + NN_b^2)$. Therefore, the time complexity of the brute-force algorithm is $O((N^3 + 2N^2N_b + N^2N_s + NN_b^2)2^{N_s})$. The greedy algorithm proposed in this paper requires that SP be found for each battery, which requires N_b iterations. Each SP can be obtained by several applications of Dijkstra's algorithms. Therefore, the total time complexity for calculating all SPs is $O(N_b(N_b + 2N_s) \log_{10} N)$. According to Appendix 1, the RBS can reconfigure $C_{N_b}^{N_{\text{set}}}$ structures by selecting N_{set} batteries from N_b batteries, which gives $\sum_{N_{\text{set}}=1}^{N_b} C_{N_b}^{N_{\text{set}}} / N_b \approx 2^{N_b} N_b^{-1}$ on average. Thus, with the bisection method, the time complexity of the greedy algorithm is $O((N^3 + 2N^2N_b + N^2N_s + NN_b^2)2^{N_b} N_b^{-1} \log_{10} N_b + N_b(N_b + 2N_s) \log_{10} N)$. Based on currently proposed RBS structures [39, 40, 41, 42, 43, 44], the number N_b of batteries, N_s of switches, and N of nodes are quantitatively related as follows: $N_s \approx (3\text{--}5)N_b$, $N \approx N_s$. After simplifying, the time complexity of the method with greedy algorithm is $O(2^{N_b} N_s^2 \log_{10} N_b)$, while it is $O(2^{N_s} N_s^3)$ for the method with brute force algorithm. Therefore, as the RBS grows, especially in the number of switches, the greedy algorithm gains an advantage over the brute-force algorithm. This is confirmed by the number of structures required to determine the MAC in the previous section. Compared with the brute-force algorithm, the method based on the greedy algorithm is 3 000 to 48 000 times more efficient, which is theoretically $N_s 2^{N_s - N_b} \log_{10} N_b$ times according to the above time-complexity analysis. This benefits from two key points:

- (1) The SPs guide the RBS to reconfigure reasonable structures rather than blindly going through all possible structures. This reduces the complexity from 2^{N_s} to 2^{N_b} , which is the main reason for the improvement in efficiency.

(2) The bisection method further accelerates this process, reducing the complexity from 2^{N_b} to $2^{N_b} N_B^{-1} \log_{10} N_b$.

Furthermore, this approach has the capability to handle RBSs with arbitrary structures, which is another significant advantage of it. It is able to correctly calculate the MACs of RBSs with arbitrary structures, even when they have different variant batteries, or even random isolated batteries. These results have been validate in the previous subsection.

However, the suggested greedy algorithm still includes exponential terms in its time complexity, indicating that it struggles to perform at scale. Additionally, all batteries are assumed to be identical for the sake of simplification in the derivation. However, there may exist a small balancing current, which could introduce a minor bias to the MAC, due to variations in open-circuit voltage u_b and internal resistance r_b in reality. Nevertheless, the proposed greedy algorithm remains a viable choice for the RBS design and optimization in the early stage, and the issue of balancing current bias can be addressed by considering the variations in batteries and replacing the internal resistance with impedance when constructing the directed graph model.

3.3.3 application scenarios

Note that η is used as the objective function instead of I_o in solving for the MAC. This choice makes the resulting MAC more reasonable and applicable in practical scenarios. As shown in Tab. 4, I_o and I_b are functions of R_o , u_b , and r_b . However, when I_o is used as the objective function, even for the same RBS structure, the MAC solution and corresponding switch states could change due to different external electrical appliances. This would increase the difficulty and uncertainty of designing the RBS structure. To eliminate this problem, the ratio $\eta = I_o / \max(I_b)$ is adopted as the objective function in our research. Recall that η reflects only the structure's ability to output current, rather than the actual current outputting by the battery system. Assuming that the MAC of batteries in the RBS is I_m , the maximum output current of the RBS structure can be calculated as ηI_m by determining the value of η for the structure.

The method proposed in this paper facilitates the design of RBSs in the following ways: most currently proposed RBS structures [39, 40, 41, 42, 43, 44] have simple topological characteristics, so calculating the MACs is relatively straightforward, even intuitive. However, these simple structures do not always fully satisfy the requirements of complex applications, such as dynamically adapting the circuit to variable and random operating conditions or actively equalizing differences between batteries in the RBS. Moreover, isolating the batteries disrupts the original regularity and symmetry of the topology, which complicates the otherwise simple structure, and the maximum output current of the system becomes more challenging to obtain. In contrast, the proposed method calculates the MAC of arbitrary RBS structures, notably the complex and flexible RBS structures.

To illustrate this point, the MACs of the RBS structure in Fig. 4c are calculated after isolating one or more of the batteries, as shown in Figs. 10a–10d. When a single battery is isolated, the RBS is still capable of outputting the maximum current, denoted as $\eta = 2$. When two batteries are isolated, there are two scenarios: one is isolating two batteries within the same substructure (Figure 10b), resulting in $\eta = 2$; the other is isolating one battery in each of the two substructures (Figure 10c),

410 resulting in $\eta = 1$. If three batteries are isolated, the RBS can only output the current of a single
411 battery, which is $\eta = 1$. Therefore, the battery management system can adjust the output current
412 and control the RBS to reconfigure the corresponding structure based on the isolated batteries.

413 4 Conclusion

414 This paper proposes a pervasive and automated method to efficiently compute the MAC of an
415 RBS. The method is implemented by a greedy algorithm combined with an improved directed graph
416 model. Not only does the method provides the same global MAC calculation results as the brute
417 force method, but it also improves the calculation efficiency by 3 000 to 48 000 times for three RBS
418 structures in the case study. Theoretically, for an RBS with N_s switches and N_b batteries, the
419 efficiency of the proposed method is $N_s 2^{N_s - N_b} \log_{10} N_b$ times that of the brute-force method, which
420 is mainly because of using the batteries' SPs to guide the RBS to reconfigure reasonable structures
421 rather than blindly going through all possible structures. The main advantage of this method is
422 its ability to calculate the MAC of RBSs with arbitrary structures. Even in scenarios with random
423 isolated batteries, the proposed method remains effective. This method helps to fully tap the current
424 output potential of the RBS, guide the RBS structure design and optimization in the design stage,
425 and assist in evaluating the current-overload risk of the system in practical applications.

426 5 Appendix

427 Acknowledgments

428 Author Contributions

429 B. Xu conceived the main idea, formulated the overarching research goals and aims, designed the
430 algorithm, and reviewed and revised the manuscript. G. Hua developed and analyzed the model,
431 implemented the code and supporting algorithms, and wrote the initial draft. C. Qian provided
432 critical review, commentary, and revisions. Q. Xia contributed to shaping the research, analysis,
433 and manuscript. B. Sun conducted the research and investigation process. Y. Ren secured the
434 funding and supervised the project. Z. Wang verified the results and provided necessary resources.

435 Conflicts of Interest

436 The authors declare that there is no conflict of interest regarding the publication of this article.

437 Data Availability

438 This work does not require any data to be declared or publicly disclosed.

Algorithm 1: Get the max available currents of a certain RBS

Data: Directed graph model $G(V, E)$ of the RBS

Result: $\max \eta$

```
1 for  $i \in E_b$  do
2    $P_i \leftarrow \{path | \text{starts at } v_1 \text{ and ends at } v_n\}$ ;
3    $SP_i \leftarrow p_i$  which has the minimum  $\omega(p_i)$  among all  $p_i \in P_i$ .
4 end
5 get  $A$  by Eq. 1;
6 while not yet determine  $\max \eta$  do
7    $N_{\text{set}} \leftarrow$  number of selected SPs calculated by dichotomy;
8    $C_b \leftarrow$  set of all combinations of  $N_{\text{set}}$  batteries from  $N_b$ ;
9   for  $c_b \in C_b$  do
10     $\mathbf{x}_s \leftarrow$  list of all switches' state:  $x_s[j] = 1$  if  $j \in \bigcup_{i \in c_b} SP_i$  else 0;
11     $\mathbf{X} \leftarrow \text{diag}[1, 1, \dots, 1, \mathbf{x}_s]$ ;
12    get  $\mathbf{Y}_n$  by Eq. 9;
13    if  $\mathbf{Y}_n$  is invertible then
14      pass
15    else
16      construct an effective solution
17    end
18    get  $I_o$  by Eq. 7;
19    get  $\mathbf{I}_b$  by Eq. 8;
20    if  $\max(\mathbf{I}_b) \leq I_m$  then
21       $\eta \leftarrow I_o / \max(\mathbf{I}_b)$ ;
22    else
23      break
24    end
25  end
26 end
```

References

- [1] Yuqing Yang, Stephen Bremner, Chris Menictas, and Merlinde Kay. Battery energy storage system size determination in renewable energy systems: A review. *Renewable and Sustainable Energy Reviews*, 91:109–125, August 2018.
- [2] Luanna Maria Silva de Siqueira and Wei Peng. Control strategy to smooth wind power output using battery energy storage system: A review. *Journal of Energy Storage*, 35:102252, March 2021.
- [3] Eugene Schwanbeck and Penni Dalton. International Space Station Lithium-ion Batteries for Primary Electric Power System. In *2019 European Space Power Conference (ESPC)*, pages 1–1. IEEE, September 2019.
- [4] Lihua Zhang. Development and Prospect of Chinese Lunar Relay Communication Satellite. *Space: Science & Technology*, 2021, January 2021.
- [5] Jaephil Cho, Sookyung Jeong, and Youngsik Kim. Commercial and research battery technologies for electrical energy storage applications. *Progress in Energy and Combustion Science*, 48:84–101, June 2015.
- [6] Naixing Yang, Xiongwen Zhang, BinBin Shang, and Guojun Li. Unbalanced discharging and aging due to temperature differences among the cells in a lithium-ion battery pack with parallel combination. *Journal of Power Sources*, 306:733–741, February 2016.
- [7] Fei Feng, Xiaosong Hu, Lin Hu, Fengling Hu, Yang Li, and Lei Zhang. Propagation mechanisms and diagnosis of parameter inconsistency within Li-Ion battery packs. *Renewable and Sustainable Energy Reviews*, 112:102–113, September 2019.
- [8] J. A. Jeevarajan and C. Winchester. Battery Safety Qualifications for Human Ratings. *Interface magazine*, 21(2):51–55, January 2012.
- [9] Daniel Vázquez Pombo. A Hybrid Power System for a Permanent Colony on Mars. *Space: Science & Technology*, 2021, January 2021.
- [10] Weiji Han, Torsten Wik, Anton Kersten, Guangzhong Dong, and Changfu Zou. Next-Generation Battery Management Systems: Dynamic Reconfiguration. *IEEE Industrial Electronics Magazine*, 14(4):20–31, December 2020.
- [11] Song Ci, Ni Lin, and Dalei Wu. Reconfigurable battery techniques and systems: A survey. *IEEE Access*, 4:1175–1189, 2016.
- [12] Nejmeddine Bouchhima, Matthias Gossen, Sascha Schulte, and Kai Peter Birke. Lifetime of self-reconfigurable batteries compared with conventional batteries. *Journal of Energy Storage*, 15:400–407, 2018.

- [13] Song Ci, Jiucui Zhang, Hamid Sharif, and Mahmoud Alahmad. A novel design of adaptive reconfigurable multicell battery for power-aware embedded networked sensing systems. In *IEEE GLOBECOM 2007-IEEE Global Telecommunications Conference*, pages 1043–1047. IEEE, 2007.
- [14] Jan Engelhardt, Tatiana Gabderakhmanova, Gunnar Rohde, and Mattia Marinelli. Reconfigurable stationary battery with adaptive cell switching for electric vehicle fast-charging. In *2020 55th International Universities Power Engineering Conference (UPEC)*, pages 1–6, 2020.
- [15] Jan Engelhardt, Jan Martin Zepter, Tatiana Gabderakhmanova, Gunnar Rohde, and Mattia Marinelli. Double-string battery system with reconfigurable cell topology operated as a fast charging station for electric vehicles. *Energies*, 14(9):2414, 2021.
- [16] H. Visairo and P. Kumar. A reconfigurable battery pack for improving power conversion efficiency in portable devices. In *2008 7th International Caribbean Conference on Devices, Circuits and Systems*, pages 1–6. IEEE, April 2008.
- [17] Barrie Lawson. A Software Configurable Battery. *EVS26 International Battery, Hybrid and Fuel Cell Electric Vehicle Symposium*, 2012.
- [18] Liang He, Linghe Kong, Siyu Lin, Shaodong Ying, Yu Gu, Tian He, and Cong Liu. Reconfiguration-assisted charging in large-scale lithium-ion battery systems. In *2014 ACM/IEEE International Conference on Cyber-Physical Systems (ICCPs)*, pages 60–71. IEEE, 2014.
- [19] Hahnsang Kim and Kang G Shin. On dynamic reconfiguration of a large-scale battery system. In *2009 15th IEEE Real-Time and Embedded Technology and Applications Symposium*, pages 87–96. IEEE, 2009.
- [20] Weiji Han and Anton Kersten. Analysis and Estimation of the Maximum Circulating Current during the Parallel Operation of Reconfigurable Battery Systems. In *2020 IEEE Transportation Electrification Conference & Expo (ITEC)*, pages 229–234. IEEE, June 2020.
- [21] Jan Engelhardt, Jan Martin Zepter, Tatiana Gabderakhmanova, Gunnar Rohde, and Mattia Marinelli. Double-String Battery System with Reconfigurable Cell Topology Operated as a Fast Charging Station for Electric Vehicles. *Energies*, 14(9):2414, 2021.
- [22] Weiji Han, Anton Kersten, Changfu Zou, Torsten Wik, Xiaoliang Huang, and Guangzhong Dong. Analysis and estimation of the maximum switch current during battery system reconfiguration. *IEEE Transactions on Industrial Electronics*, 69(6):5931–5941, 2021.
- [23] Lidiya Komsijska, Tobias Buchberger, Simon Diehl, Moritz Ehrensberger, Christian Hanzl, Christoph Hartmann, Markus Hölzle, Jan Kleiner, Meinert Lewerenz, Bernhard Liebhart, Michael Schmid, Dominik Schneider, Sascha Speer, Julia Stöttner, Christoph Terbrack, Michael Hinterberger, and Christian Endisch. Critical Review of Intelligent Battery Systems: Challenges, Implementation, and Potential for Electric Vehicles. *Energies*, 14(18):5989, 2021.

- [24] Luis D. Couto and Michel Kinnaert. Partition-based Unscented Kalman Filter for Reconfigurable Battery Pack State Estimation using an Electrochemical Model. In *2018 Annual American Control Conference (ACC)*, pages 3122–3128. IEEE, June 2018.
- [25] Anton Kersten, Manuel Kuder, Weiji Han, Torbjorn Thiringer, Anton Lesnicar, Thomas Weyh, and Richard Eckerle. Online and On-Board Battery Impedance Estimation of Battery Cells, Modules or Packs in a Reconfigurable Battery System or Multilevel Inverter. In *IECON 2020 The 46th Annual Conference of the IEEE Industrial Electronics Society*, pages 1884–1891. IEEE, October 2020.
- [26] Michael Schmid, Emanuel Gebauer, Christian Hanzl, and Christian Endisch. Active Model-Based Fault Diagnosis in Reconfigurable Battery Systems. *IEEE Transactions on Power Electronics*, 36(3):2584–2597, March 2021.
- [27] Jan Kacatl, Jingyang Fang, Tomas Kacatl, Nima Tashakor, and Stefan Goetz. Design and Analysis of Modular Multilevel Reconfigurable Battery Converters for Variable Bus Voltage Powertrains. *IEEE Transactions on Power Electronics*, 38(1):130–142, January 2023.
- [28] Feng Yang, Fei Gao, Baochang Liu, and Song Ci. An Adaptive Control Framework for Dynamically Reconfigurable Battery Systems Based on Deep Reinforcement Learning. *IEEE Transactions on Industrial Electronics*, 69(12):12980–12987, December 2022.
- [29] Weiji Han, Changfu Zou, Liang Zhang, Quan Ouyang, and Torsten Wik. Near-Fastest Battery Balancing by Cell/Module Reconfiguration. *IEEE Transactions on Smart Grid*, 10(6):6954–6964, November 2019.
- [30] Xinghua Liu, Guoyi Chang, Jiaqiang Tian, Zhongbao Wei, Xu Zhang, and Peng Wang. Flexible path planning-based reconfiguration strategy for maximum capacity utilization of battery pack. *Journal of Energy Chemistry*, 86:362–372, November 2023.
- [31] Si-Zhe Chen, Yule Wang, Guidong Zhang, Le Chang, and Yun Zhang. Sneak Circuit Theory Based Approach to Avoiding Short-Circuit Paths in Reconfigurable Battery Systems. *IEEE Transactions on Industrial Electronics*, 68(12):12353–12363, 2021.
- [32] Kailong Liu, Zhongbao Wei, Chenghui Zhang, Yunlong Shang, Remus Teodorescu, and Qing-Long Han. Towards Long Lifetime Battery: AI-Based Manufacturing and Management. *IEEE/CAA Journal of Automatica Sinica*, 9(7):1139–1165, July 2022.
- [33] Morteza Mollajafari. An efficient lightweight algorithm for scheduling tasks onto dynamically reconfigurable hardware using graph-oriented simulated annealing. *Neural Computing and Applications*, 35(24):18035–18057, August 2023.
- [34] Liang He, Linghe Kong, Siyu Lin, Shaodong Ying, Yu Gu, Tian He, and Cong Liu. Reconfiguration-assisted charging in large-scale Lithium-ion battery systems. In *2014 ACM/IEEE International Conference on Cyber-Physical Systems (ICCPS)*, pages 60–71. IEEE, April 2014.

- [35] Zoltan Mark Pinter, Dimitrios Papageorgiou, Gunnar Rohde, Mattia Marinelli, and Chresten Traholt. Review of Control Algorithms for Reconfigurable Battery Systems with an Industrial Example. In *2021 56th International Universities Power Engineering Conference (UPEC)*, pages 1–6, August 2021.
- [36] Liang He, Lipeng Gu, Linghe Kong, Yu Gu, Cong Liu, and Tian He. Exploring Adaptive Reconfiguration to Optimize Energy Efficiency in Large-Scale Battery Systems. In *2013 IEEE 34th Real-Time Systems Symposium*, pages 118–127, December 2013.
- [37] Hongwen He, Rui Xiong, Xiaowei Zhang, Fengchun Sun, and JinXin Fan. State-of-Charge Estimation of the Lithium-Ion Battery Using an Adaptive Extended Kalman Filter Based on an Improved Thevenin Model. *IEEE Transactions on Vehicular Technology*, 60(4):1461–1469, May 2011.
- [38] S.M. Mousavi G. and M. Nikdel. Various battery models for various simulation studies and applications. *Renewable and Sustainable Energy Reviews*, 32:477–485, April 2014.
- [39] Song Ci, Jiucui Zhang, Hamid Sharif, and Mahmoud Alahmad. A Novel Design of Adaptive Reconfigurable Multicell Battery for Power-Aware Embedded Networked Sensing Systems. In *IEEE GLOBECOM 2007-2007 IEEE Global Telecommunications Conference*, pages 1043–1047, November 2007.
- [40] Mahmoud Alahmad, Herb Hess, Mohammad Mojarradi, William West, and Jay Whitacre. Battery switch array system with application for JPL’s rechargeable micro-scale batteries. *Journal of Power Sources*, 177(2):566–578, March 2008.
- [41] Hahnsang Kim and Kang G. Shin. Dependable, efficient, scalable architecture for management of large-scale batteries. In *Proceedings of the 1st ACM/IEEE International Conference on Cyber-Physical Systems*, ICCPS ’10, pages 178–187, New York, NY, USA, April 2010. Association for Computing Machinery.
- [42] Younghyun Kim, Sangyoung Park, Yanzhi Wang, Qing Xie, Naehyuck Chang, Massimo Poncino, and Massoud Pedram. Balanced reconfiguration of storage banks in a hybrid electrical energy storage system. In *2011 IEEE/ACM International Conference on Computer-Aided Design (ICCAD)*, pages 624–631, November 2011.
- [43] Taesic Kim, Wei Qiao, and Liyan Qu. A series-connected self-reconfigurable multicell battery capable of safe and effective charging/discharging and balancing operations. In *2012 Twenty-Seventh Annual IEEE Applied Power Electronics Conference and Exposition (APEC)*, pages 2259–2264, February 2012.
- [44] Liang He, Linghe Kong, Siyu Lin, Shaodong Ying, Yu Gu, Tian He, and Cong Liu. Reconfiguration-assisted charging in large-scale Lithium-ion battery systems. In *2014 ACM/IEEE International Conference on Cyber-Physical Systems (ICCPs)*, pages 60–71, April 2014.